Research Square

Preprints are preliminary reports that have not undergone peer review.
They should not be considered conclusive, used to inform clinical practice,
or referenced by the media as validated information.

Tracking skeletal change in dead coral colonies: A non-invasive 3D photogrammetry workflow and case-study application

Nicolas Mafla Viscarra

n.viscarra@aims.gov.au

Australian Institute of Marine Science

Emma Kennedy

Australian Institute of Marine Science

Maren Toor

Australian Institute of Marine Science

Marine Lechene

Australian Institute of Marine Science

Sophie Gordon

Australian Institute of Marine Science

Renata Ferrari

Australian Institute of Marine Science

Research Article

Keywords:

Posted Date: November 11th, 2026

DOI: https://doi.org/10.21203/rs.3.rs-11692986/v1

License: This work is licensed under a Creative Commons Attribution 4.0 International License.
Read Full License

Additional Declarations: No competing interests reported.

Manuscript title: Tracking skeletal change in dead coral colonies: A non-invasive 3D photogrammetry workflow and case-study application

Author full names: Nicolas Mafla Viscarra[1], Emma Kennedy[1], Maren Toor[1], Marine Lechene[1], Sophie Gordon[1], Renata Ferrari[1]

Institutions and addresses: Australian Institute of Marine Science, Townsville, QLD 4810, Australia[1]

Correspondence: Nicolas Mafla Viscarra, email: n.viscarra@aims.gov.au

ORCiD: 0009-0005-5814-9072 (Nicolas Mafla Viscarra), 0000-0003-1821-9740 (Emma Kennedy), 0009-0004-9458-877X (Maren Toor), 0000-0002-5278-4332 (Marine Lechene), 0000-0003-1775-7221 (Sophie Gordon), 0000-0002-5056-1178 (Renata Ferrari)

Statements and Declarations

Competing Interests and Funding: The authors declare that they have no known competing financial interests or personal relationships that could have appeared to influence the work reported in this paper.

Acknowledgements: This work was undertaken by the Ecological Intelligence for Reef Restoration and Adaptation subprogram (EcoRRAP) of the Reef Restoration and Adaptation Program (RRAP). Funded by the partnership between the Australian Governments Reef Trust and the Great Barrier Reef Foundation. The RRAP partners and authors of this wok acknowledge Aboriginal and Torres Strait Islander Peoples as the first marine scientists and carers of Country. We specifically acknowledge and thank the following Traditional Owners of sea Country that this manuscript relates to: Woppaburra, Bailai, Gurang, Gooreng Gooreng, Taribelang Bunda.

Author contributions: Renata Ferrari and Emma Kennedy conceived the ideas; Renata Ferrari, Nicolas Mafla Viscarra, Maren Toor and Marine Lechene designed methodology; Sophie Gordon participated to the data collection and curation; Renata Ferrari and Emma Kennedy supervised the research; Nicolas Mafla Viscarra conducted the data analysis, visualisation and writing of the original draft. Renata Ferrari, Nicolas Mafla-Viscarra and Emma Kennedy contributed critically to the drafts and gave final approval for publication.

ABSTRACT

The breakdown of coral structures by bioeroding organisms is a key reef process. Understanding how reef material is lost over time is increasingly important as reefs degrade under climate change. Quantifying bioerosion at the colony scale requires repeated observations of recently dead coral skeletons through time. Large-area photogrammetry offers a reliable, non-invasive approach, allowing thousands of colonies to be tracked simultaneously across repeated surveys. Here, we present a protocol to quantify structural changes from surficial bioerosion and overgrowth in coral skeletons using 3D reconstructions from large-area photogrammetry. The workflow identifies recently dead colonies, extracts the corresponding image subsets, and reconstructs sub-millimetre-resolution 3D models of individual skeletons. Models from the first survey (2022) were aligned with those from the second (2023) and compared using the Geomagic 3D compare tool. To assess precision, we randomly selected 10 skeletons and generated 10 independent reconstructions of each, then compared variation in estimated volume and surface area. Precision varied among morphologies. For surface area, relative standard error (RSE) was lowest for tabular Acropora (0.22–0.31%) and highest for branching non-Acropora (1.20–5.07%). Volume estimates followed the same pattern, with RSE of 0.22–1.78% for tabular Acropora and 2.48–5.97% for branching non-Acropora. We applied the protocol to 60 skeletons from the southern Great Barrier Reef between May 2022 and May 2023. Erosion and deposition rates differed among morphotaxa, with branching non-Acropora skeletons eroding significantly faster. This approach enables repeatable quantification of change in coral skeleton structure and provides a scalable tool for assessing reef degradation.

Key words: Bioerosion, 3D modelling, external coral skeleton erosion, photogrammetry, surface deposition, topographic complexity.

1. INTRODUCTION

The Great Barrier Reef spans 345,000 km^2, sustains over 60,000 jobs (Marsden et al., 2017), and is widely regarded as one of the best-managed reef systems globally. However, it continues to face multiple pressures, including crown-of-thorns starfish (COTS) outbreaks, cyclones, and climate change-induced coral bleaching, all of which contribute to coral mortality (Bruno & Selig, 2007; Deaker & Byrne, 2022; Hughes et al., 2011, 2017). As these pressures intensify, understanding how dead coral structures change through time is becoming increasingly important. Increasing coral mortality expands the amount of dead reef substrate available

for erosion and colonisation, while also increasing the contribution of dead skeletons to benthic habitat structure and overall reef topographical complexity.

Topographical complexity refers to the three-dimensional variation in the physical structure of the reef surface (height, slope, rugosity, surface area and void space). It plays a vital role in reef functioning and resilience, with more complex surfaces providing greater habitat and refuges for fish and invertebrates, enhancing larval settlement, and dissipating wave energy, all of which contribute to reef stability and biodiversity (Graham & Nash, 2013).

Reef topographical complexity arises from the balance between constructional processes, like carbonate accretion, and erosional processes, including bioerosion (Perry et al., 2013). Following coral mortality, skeletal remains may undergo chemical, physical, and biological erosion, or experience increases in volume due to algal overgrowth, sediment accumulation or other surface deposition (Eakin, 2001a; Molina-Hernández et al., 2022). Grazing by sea urchins and parrotfishes can be major drivers of erosion, while epilithic and endolithic algae and cyanobacteria are typically among the first colonizers of newly exposed coral skeletons (Estrada-Saldívar et al., 2020; Taylor et al., 2020). Rates and trajectories of post-mortality structural change are likely to vary among coral morphologies, highlighting the importance of assessing skeletal dynamics at the colony level.

Traditional methods for quantifying structural complexity are often technically demanding and limited in their application (Risk, 1972), while commonly used methods for measuring erosion and accretion, such as the buoyant weight method, can be invasive and destructive (Ferrari et al., 2017a). In contrast, photogrammetry provides an emerging, non-invasive approach for measuring reef and coral colony structure across ecologically relevant scales.

Large-area photogrammetry allows rapid, non-invasive measurement of coral colony attributes across thousands of individuals spanning broad and environmentally varied reef areas (Álvarez-Noriega et al., 2025). Survey areas typically range from 10 to 1,000 m^2, with researchers often employing permanent plots to track changes in coral communities over time (Álvarez-Noriega et al., 2025; Kopecky et al., 2024). As a result, photogrammetry is increasingly being adopted as an alternative to labour-intensive manual data extraction in complex reef environments (Remmers et al., 2025). However, photogrammetric surveys involve an inherent trade-off between the covered spatial extent and the resolution of the resulting 3D models (Figueira et al., 2015). This trade-off may limit the precision with which the images from large-area 3D models can be used to reconstruct individual coral skeletons and detect changes in volume and surface area though time.

The aim of this study is to develop and validate a non-invasive protocol for quantifying temporal structural change in coral skeletons using reef-scale photogrammetry. The protocol uses large area 3D reef reconstructions to identify recently dead coral colonies, extract targeted image subsets, and generate high-resolution 3D models of individual coral skeletons. We also establish a simple approach for assessing methodological precision in 3D volume and surface area comparisons. To demonstrate the application of the protocol, we reconstruct coral skeletons at two time points and quantify 3D deviations, as well as percentage changes in volume and surface area, for 60 skeletons over 12 months. Because dead coral skeletons can undergo both material loss and surface accumulation, we expected to detect not only structural loss due to erosion, but also potential increases in volume and surface area associated with algal overgrowth or sediment deposition on the skeletons.

2. MATERIALS AND METHODS

To quantify skeletal change on death coral colonies, we developed a non-invasive 3D workflow combining large-scale photogrammetry, coral classification and image filtering, and individual coral skeleton reconstruction for a later extraction and analysis of structural metrics (Fig. 1).

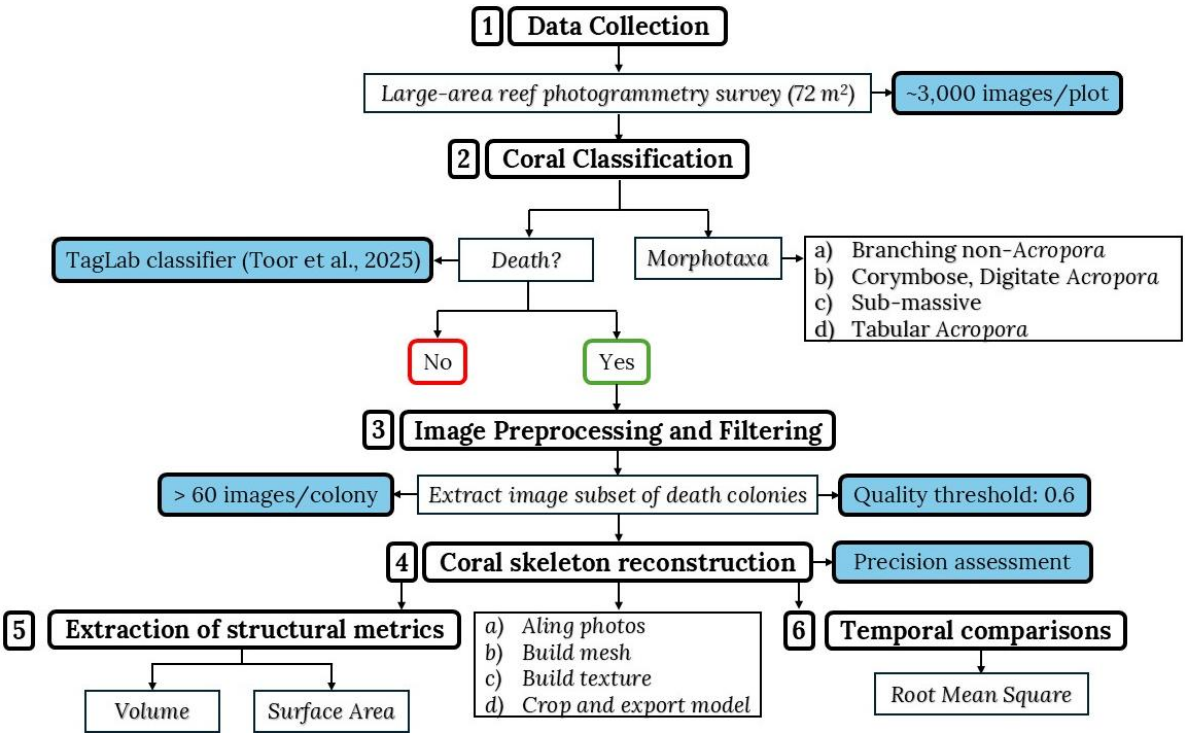


Fig. 1 Conceptual diagram of the non-invasive 3D reconstruction protocol to measure skeletal change in dead coral colonies

2.1. Data Collection and Coral Classification

Images were collected from 29 permanent plots across 10 sampling sites on two reefs in the Capricorn-Bunker Group of the southern Great Barrier Reef in May 2022 and May 2023 (Fig. 2). Each plot measured 12 x 6 meters (72 m^2) and comprised approximately 2,500 - 3,600 high-quality images.

At Heron Island Reef, plots were located across two depth zones: shallow reef slopes (3-8 meters) and deeper reef slopes (9–15 meters) and included both sheltered (6 plots) and exposed (12 plots) reef slope environments. At Lady Musgrave Reef, imaging was conducted in shallow habitats only, including sheltered slopes (2 plots), exposed slopes (6 plots), and lagoon (3 plots) reef environments. Recently dead coral colonies, defined as those that died since the previous survey, were randomly selected from each plot for individual 3D reconstruction.

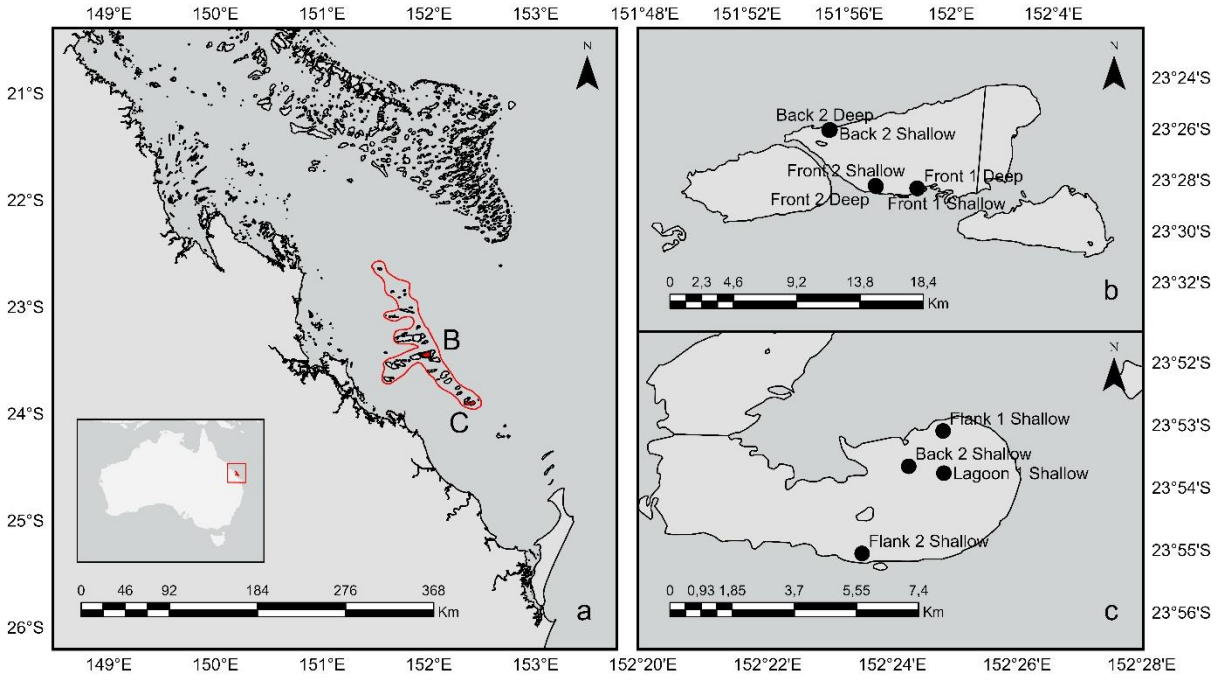


Fig. 2 Map showing the location of the two studied reefs: Heron Island (b) and Lady Musgrave (c), located in the Southern Great Barrier Reef, Australia (a)

Following Aston et al. (2022), we used a morphotaxa-based approach to classify the coral colonies examined in this study. Across both years, 14 coral species representing 4 distinct morphotaxa were identified: tabular *Acropora*, corymbose, digitate *Acropora*, branching non-*Acropora* and sub-massive corals (Table 1). In total, 60 paired coral skeleton reconstructions were successfully generated for temporal comparison.

Table 1 Studied species and morphotaxa description. Number of dead colonies (n) are specified, as well as morphotaxa abbreviations.

Taxa	Abbrev.	Morphotaxa	n	Description
A. cytherea	Acyt	Tabular *Acropora*	15	Colonies characterized by flat, table-like structures with horizontal growth.
A. hyacinthus	Ahya			
A. solitaryensis	Asol			
Acropora sp.	Atab			
A. corymbose	Acor	Corymbose, Digitate *Acropora*	32	Dense, bushy, growth forms.
Acropora sp.	Adgt			
A. humilis	Ahum			
A. abrotanoides	Aabr			
A. tenuis	Aten			
P. damicornis	Pdam	Branching non-*Acropora*	10	Dense, bushy, growth forms that reproduce predominately via broadcast spawning.
S. hystrix	Shys			
S. pistillata	Spis			
G. edwardsi	Gedw	Sub-massive	3	Semi-spherical shaped colonies.
Platygyra sp.	Plat			

2.2. Field and Computational Equipment

Images were captured using a Nikon D850 DSLR camera (Nikon Corporation), equipped with a 20 mm Nikon NIKKOR lens. Camera settings were aperture f/11, shutter speed 1/200 s, ISO 200, and manual white balance adjusted for underwater conditions. Each image was recorded in JPEG format, with a file size of approximately 20.3 MB.

Data processing was conducted on a workstation with an Intel(R) Xeon(R) W-2245 CPU 3.91 GHz processor and 128 GB of RAM. TagLab and ArcGIS Pro 3.3.1 were used to inspect the orthomosaic of each plot, identify recently dead coral colonies, and track colonies through time. Agisoft Metashape Professional 1.7.6 was used to create 3D reconstructions of individual coral skeletons and Geomagic Control 2015 was used for temporal comparisons and extraction of bioerosion-related structural metrics. Further details on the broader photogrammetric and image analysis workflow are provided in Gordon et al. (2023, 2024) and Toor et al. (2025).

2.3. Image Preprocessing and Filtering

A subset of photographs was selected from each plot to reconstruct individual dead coral colonies. This process required a series of cleaning and preprocessing steps before initiating the 3D model reconstruction (Table 2). Recently dead coral colonies were first identified using TagLab (v2022.02.11–v2025.2.15), focusing on colonies that were alive in the survey conducted prior to this study (2021), and classified as dead in 2022. This classification involves an automatic digitisation of dead coral colonies in TagLab which consists of three steps: (1) preparation of the training data, (2) training of the classifier, and (3) running the classifier (Toor et al., 2025). The classifier defined dead colonies as skeletons exhibiting 100% mortality while retaining visible skeletal structure. These selected skeletons were then reconstructed again for the 2023 survey to quantify structural change over 12 months, by comparing both models in Geomagic Control.

Candidate skeletons were visually inspected in ArcGIS Pro, and the corresponding images were filtered from the full plot dataset in Agisoft Metashape Pro. A second filtering step was applied, retaining only images with a quality score of 0.6 or higher to ensure the highest resolution for the reconstruction process. However, if fewer than 60 images remained after the second filtering process, the filter was not applied. This threshold was maintained because a baseline of 60–80 images is recommended to achieve optimal reconstruction quality. Following image selection, the alignment process was performed using the filtered images. Subsequently, camera parameters were optimized to enhance accuracy, and the working region was resized as necessary to focus on the targeted colony, rather than the entire original plot.

Table 2 Metashape Pro v 1.7.6 preprocessing steps: Photo setup, alignment and error reduction. Lange & Perry (2020) methodology was used as a reference for this part of our work.

Workflow Step	Description
Free-Form (Lasso) Selection Tool	Using the Cloud View of the 3D model for each plot, the tie points associated with the identified dead colony were carefully selected.
Filter picture by tie points	Right click on the selected area and select filter by tie points. Move the filtered images to a new chunk. We recommend between 60-80 images per colony.
Estimate Image Quality	Right click at any photo on the photo view panel and select estimate image quality. Select all the cameras. Eliminate those images with less than 0.6 image quality.

	Apply this filter only if the remaining dataset contains between 60 and 80 images. Change the images file path accordingly.
Align Photos	*General settings:* Accuracy: Highest, Check Generic Preselection, Key point limit: 40,000, Tie point limit: 4,000, Apply masks to: None, Check Reset current alignment. *Advanced:* by default.
Optimize Cameras	Check all except k4, b1, b2, p3, p4 (default)

165

166 **2.4. Coral skeleton reconstruction**

167 After resizing the working region, the photographs for each dead coral colony, the 3D reconstruction
168 process was conducted in Metashape Pro v 1.7.6 (Table 3). The Build Mesh and Build Texture steps were
169 performed using a semi-automatic batch process, which streamlined the workflow by integrating each step into
170 the desired sequence and consistently applying specified settings across all chunks. Identical workflows and
171 parameters were used for images from both study years to ensure comparability. To verify the model's spatial
172 accuracy, two markers were placed on the digital model, and a scale bar was generated based on the known
173 physical distance between them. The reconstructed model and point cloud were cropped to isolate the specific
174 area of study, removing surrounding reef data irrelevant for this project. The bounding box was then resized to
175 constrain the final output region. The completed 3D models were saved and exported in OBJ. format for further
176 analysis in Geomagic.

177

178 **Table 3** Metashape Pro 3D modeling steps: Reconstruction and export To optimize 3D models of coral
179 skeletons, rather than live coral colonies, the following settings used in this study were modified from the ones
180 applied for similar 3D modelling purposes (Aston et al., 2022; Lange & Perry, 2020).

Workflow step	**Description**
Build Mesh	*General settings*: Source data: Depth Map, Surface type: Arbitrary (3D), Depth Maps Quality: Ultra-high, Face count: High. *Advanced*: Interpolation: Enabled (default), Check Calculate vertex colors.
Build Texture	*General Settings*: Mapping mode: Generic, Blending mode: Mosaic (default), Texture size/count: 8,192 x 2. *Advanced*: Check Enable hole filling and Enable ghosting filter.

Create scale bar	Identify a physical marker within the reconstructed model. Create a scale bar between two marker points, then add the known distance between them (0.3 m for this project). Click the update button (circular arrows) on the reference pane toolbar.
Crop model and point cloud	Select and crop the area of interest within the reconstructed model and point cloud. Click on the region tool on the top toolbar (Resize Bounding Box: Fit-to-shape)
Save and export project	Export model as .obj file format.

2.5. Precision assessment of 3D reconstructions

To assess the precision of our methodology, we randomly selected 10 coral skeletons from the study dataset and reconstructed them 10 times for the same year, following the exact same procedure and parameters used in Metashape for all other corals. However, because image filtering was not standardized, i.e., we used the free-form (lasso) selection tool to manually select tie points defining the colony in the original plot model, and then filtered images based on that selection, the final set of images used for each reconstruction differed slightly. We did this, because when comparing across years, it is necessary to use this manual step, rather than an automated bounding box, to ensure adequate selection and quality assurance purposes. Thus, the purpose of this precision assessment was to replicate any potential error when comparing across years. We then compared the ten replicate models in Geomagic Control, analysed their 3D deviation using the 3D Compare tool, and computed volume and surface area metrics, to finally calculate a mean and relative standard error (RSE) values. For the 3D Compare analysis, the first version of each skeleton was used as the reference model, while versions 2–10 were used as test models, resulting in a total of nine 3D deviation heatmaps for each skeleton.

2.6. Temporal comparisons between 3D models

The 3D models from both study years for the same coral colony were imported into Geomagic Control 2015. They were first aligned using the N-Point Alignment tool, in the Alignment menu in Geomagic Control, selecting between 5 and 7 common points for both models. A pre-cleaning process was performed using the Mesh Doctor tool (Polygons menu) to remove any floating particles around the area of interest (Table 4). Additional cleaning was carried out to isolate the dead coral colony, removing surrounding reef areas with the Free-Form

(Lasso) Selection Tool. To ensure optimal quality before the temporal comparison, the Mesh Doctor tool was applied once more.

Table 4 Geomagic Control temporal comparison workflow: the Mesh Doctor, N-Point Alignment, Best-Fit Alignment, and 3D Compare tools were applied to each pair of dead colony reconstructions.

Workflow step	Description
Model import	Dead colony reconstructions for 2022 and 2023 were imported into Geomagic Control in .OBJ format
N-Point Alignment	Five to seven common points were selected in both reconstructions. The software splits the screen, and each point pair is selected sequentially: first in the reference model (earliest year) and then in the test model (latest year).
Mesh Doctor	*Operation type*: Auto-repair. *Advanced*: Dynamic Update and Clear Selection When Finished enabled; spike sensitivity set to 50%; region expansion set to 2 layers. Default values were retained for maximum small component size, maximum small tunnel size, and maximum small hole circumference.
Best-fit alignment	Sample size: 7,000 - 10,000; Tolerance: default value, Probe radius: 0.2-0.3 cm. Enable high precision fitting.
Fill All	Automatically fills gaps present in the 3D model. Uncheck: ignore complex holes and automation options. Optionally, a maximum hole circumference can be specified.
Crop models	Simultaneously crop both 3D reconstructions by using the freeform (lasso) selection tool and pressing the delete key. Focus on removing the bottom portions of the skeletons, as comparisons in these areas tend to be less reliable. Apply Mesh Doctor and Fill All tools after this step (same settings as above).
3D Compare	Deviation type: 3D deviation, Max. Deviation: 0.2 – 0.5 cm, Critical Angle: 15° - 30°. Display resolution: fine, Color averaging: 2. Color segments: 10-14.

Following this, the Best-Fit Alignment tool, located in the Alignment menu of Geomagic Control, was applied to ensure optimal alignment between models from both years. Once the alignment was visually confirmed to be satisfactory, the models were cropped simultaneously to ensure that subsequent temporal comparisons were conducted under the same conditions for both years. Mesh doctor and Fill All tools was applied for a final time. Then, the 3D Compare analysis (Analysis menu) was performed. The resulting values for average mean deviation (both positive and negative), standard deviation, and RMS (Root Mean Square: a statistical measure that calculates the square root of the average of the squared deviations between corresponding points on the models) were then saved to a spreadsheet for further analysis.

2.7. Extraction of structural metrics

Volume and surface area were computed in Geomagic, using the compute area and compute volume options within the Analysis menu. This step was repeated for each 3D model across the two studied year. The differences in volume and surface area were then calculated to determine whether skeletons experienced erosion (a decrease in volume and surface area) or an increase due to algal growth or sediment deposition. This difference was standardized by dividing it by the initial size measurement (volume or surface area) recorded in 2022. If either the 2021 or 2022 model in a pair was poorly reconstructed in Agisoft Metashape, indicated by visibly low quality in the texture of the model, the comparison in Geomagic was not performed, as the resulting volume or surface area calculations would be unreliable for comparison. Skeletons located at the edges of the plot or covered by larger corals typically yield lower quality reconstructions, whereas skeletons positioned near the centre and top of the plot generally produce higher quality models and more reliable estimations. To enhance measurement precision, a reference plane was created (Feature Menu). This isolated the upper portion of the skeleton for analysis, omitting the less reliable lower structure.

2.8. Statistical analysis

To assess the effect of coral morphology (taxa) on changes in coral skeleton structure between 2022 and 2023, we fitted separate linear mixed-effects models (LMMs) using Gaussian error distributions. Response variables included: mean 3D deviation between paired skeleton reconstructions (3D), percentage change in volume (PCV), and percentage change in surface area (PCSA), calculated for each paired colony. For the 3D deviation variable, we ran separate models using two different metrics from the 3D Compare tool: AVET (Average

Signed Error), which indicates the direction of deviation between the reference and test surfaces, and RMS (Root Mean Square), a standardized measure of the overall magnitude of deviations regardless of direction. Coral morphology, exposure level, and depth were included as fixed effects, as these factors are expected to influence skeletal changes. Reef and site were included as random intercepts to account for potential non-independence among colonies sampled within the same groups:

$$\Delta Response_i = \beta_0 + \beta_1 taxa + \beta_2 exposure + \beta_3\, depth + (1|\, reef) + (1|\, site) + \varepsilon_i$$

$$where\ Response\ is\ surface\ area, volume, or\ 3D\ deviations$$

Model assumptions were evaluated using visual inspection of residuals, Shapiro–Wilk tests for normality, and Levene's tests for homogeneity of variance. Separate models were fitted for each response variable using the same fixed and random effect's structure. Statistical analyses were conducted in R (version 4.4.2). Data were imported using the *readxl* package (Wickham & Bryan, 2024), reshaped and manipulated with *dplyr* and *tidyr* (Wickham, François, et al., 2023; Wickham, Vaughan, et al., 2023), visualised using *ggplot2* (Wickham et al., 2024), and data diagnostics and analyses were performed using the *car*, lme4, and *FSA* packages (Bates et al., 2015; Fox & Weisberg, 2023; Ogle et al., 2024).

2.9 Data and code availability

For peer review, the data and R code used in this study are available at: https://anonymous.4open.science/r/Tracking-skeletal-change-in-dead-coral-colonies-B0B5/README.md. Upon acceptance, they will be archived in a public repository.

3. RESULTS

3.1. Model reconstruction workflow

The methodology for this study was guided by previous research (Aston et al., 2022; Ferrari et al., 2017a; Lange & Perry, 2020). Few studies have reconstructed individual coral skeletons using images subsets derived from larger reef-scale reconstructions. As such, evaluating the time required for each step of the workflow is essential, providing a key reference for future studies in this field (Table 4). The complete workflow for colony reconstruction involved image preprocessing, filtering, model reconstruction, and export, with an average total processing time of 78 minutes. Image preprocessing and filtering steps, including aligning photos and optimizing

cameras, took approximately 25 minutes, while colony reconstruction and model export, including mesh and texture building, required around 52 minutes (Table 4).

Table 5 The complete workflow steps, including image preprocessing, filtering, colony reconstruction, and model export, are presented along with the time required for each step. Average times for each stage are calculated based on all the models reconstructed in this project. Most of this time was computer time, not manual human time.

Steps	Metashape Menu	Action / Tool	Time (min)
Image Preprocessing and Filtering			
1	Main Menu – Tools bar	Free-Form Selection Tool	1
2	Main Panel – right click selected points	Filter picture by tie points	1
3	Photo Panel (right click on any photo)	Estimate Image Quality	2
4	Main Menu – Workflow	Align Photos	20
5	Reference Panel	Optimize Cameras	1
Colony reconstruction and model export			
6	Main Panel	Resize Region	1
7	Main Menu – Workflow	Build Mesh	30
8	Main Menu – Workflow	Build Texture	20
9	Main Menu – Tools bar	Ruler (Tool bar)	1
10	Reference Panel	Save and export project	1
Total processing time			78

3.2. Precision assessment of 3D reconstructions

The precision assessment evaluated the reliability of the workflow for estimating skeletal surface area and volume changes. Ten randomly selected coral skeletons were each reconstructed 10 times using the same workflow, and variation among replicate reconstructions summarized using relative standard error (RSE).

3.2.1. Surface Area

Surface area estimates showed high repeatability across replicate reconstructions, although precision varied among colonies and morphotaxa. The lowest variation was observed on tabular *Acropora* skeletons, with

RSE values ranging from 0.22 - 0.31%. Branching non-*Acropora* skeletons showed RSE values of 1.20 - 4.32%, while corymbose, digitate *Acropora* morphologies ranged from 0.23 - 5.07% (Table 6).

Table 6 Mean skeletal surface area measurements for 3 coral morphologies. Values are presented as sample size (n), mean surface area ($\bar{x}$, cm²), standard error (SE), and relative standard error (RSE%).

Morpohology	Skeleton	Surface Area (cm²)			
		n	$\bar{x}$	*SE*	*RSE%*
Branching non-*Acropora*	Pdam13	10	269.3	3.24	1.20
	Pdam64	10	621.40	10.67	1.72
	Spis22	10	1,218.3	52.62	4.32
Corymbose, Digitate *Acropora*	Acor10	10	975.10	49.44	5.07
	Acor26	10	194.5	0.45	0.23
	Acor37.1	10	1,483.9	29.17	1.97
	Acor37.2	10	118.7	0.63	0.53
	Acor55	10	2,600.7	70.51	2.71
Tabular *Acropora*	Atab54	10	2,296.20	5.15	0.22
	Atab192	10	6,550.0	19.99	0.31

Tabular *Acropora* also had the largest measured surface areas among the precision-assessment colonies, ranging from 2,296.20 cm^2 (± 5.15 SE) to 6,550.0 cm^2 (± 19.99 SE). Smaller surface areas were observed on branching non-*Acropora* and corymbose, digitate *Acropora* colonies, with the smallest colonies having surface areas of 269.3 cm^2 (± 3.24 SE) and 118.7 cm^2 (± 0.63 SE), respectively (Fig. 3).

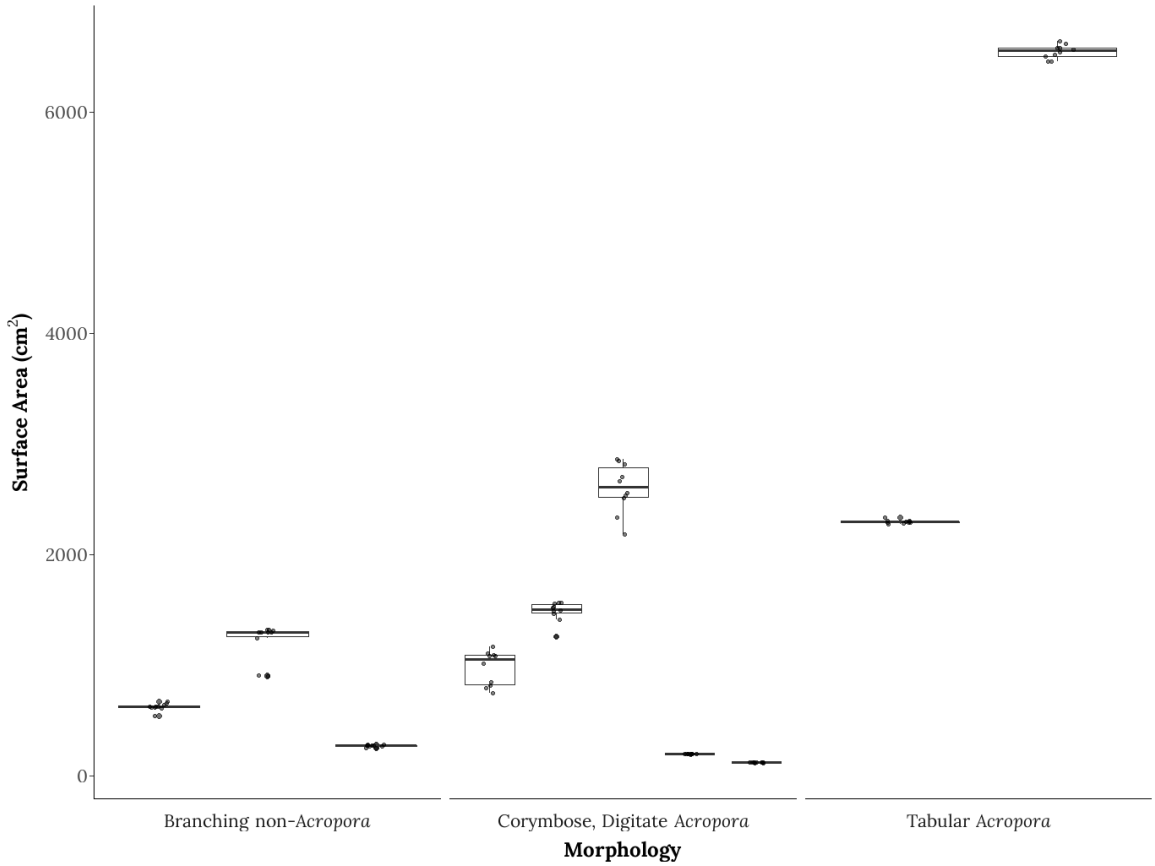


Fig. 3 Boxplot comparing mean coral surface area (cm^2) ± SE, across three distinct growth morphologies: Branching non-*Acropora* (n = 3), Corymbose, Digitate *Acropora* (n = 5), and Tabular *Acropora* (n = 2)

3.2.2. Volume

Volume estimates also showed high repeatability, with RSE values generally below 6% across all replicate reconstructions. Tabular *Acropora* skeletons showed RSE values between 1.21 – 1.78%, while branching non-*Acropora* also reported relatively low RSE values, from 1.10 – 3.15%. Corymbose, Digitate *Acropora* skeletons presented the highest variability for this metric, with RSE values ranging from 0.12 – 5.97%.

Table 7 Mean skeletal volume measurements for 3 coral morphologies. Values are presented as sample size (n), mean volume ($\bar{x}$, cm^3), standard error (SE), and relative standard error (RSE%).

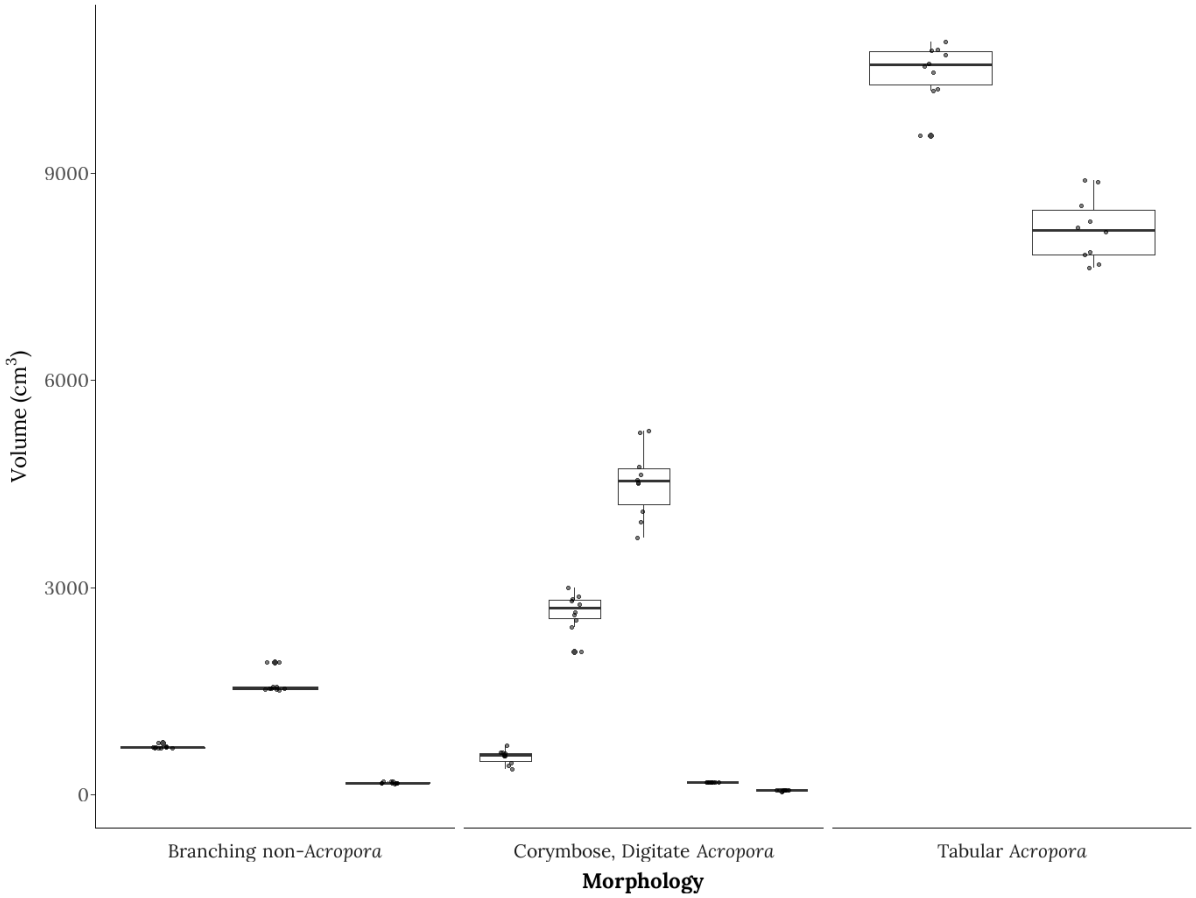
Morpohology	Skeleton	Volume (cm^3)			
		n	$\bar{x}$	*SE*	*RSE%*
Branching non-*Acropora*	Pdam13	10	174.90	4.34	2.48
	Pdam64	10	690.30	7.62	1.10

	Spis22	10	1,614.20	50.92	3.15
Corymbose, Digitate *Acropora*	Acor10	10	546.30	32.63	5.97
	Acor26	10	178.71	0.21	0.12
	Acor37.1	10	2,652.20	84.26	3.18
	Acor37.2	10	66.00	0.91	1.37
	Acor55	10	4,522.00	159.57	3.53
Tabular *Acropora*	Atab54	10	10,466.60	127.11	1.21
	Atab192	10	8,189.51	146.04	1.78

315

316 Similarly to the surface area calculations, the highest volume values were registered for the tabular
317 *Acropora* skeletons, with values between 8,189.51 cm^3 (± 146.04 SE) and 10,466.60 cm^3 (± 127.11 SE). In
318 contrast, the lower volume values were exhibited by Branching non-*Acropora* and Corymbose, Digitate
319 *Acropora* colonies, with values of 174.90 cm^3 (± 4.34 SE) and 66.00 cm^3 (± 0.91 SE), respectively (Fig. 4).

320



321

322 **Fig. 4** Boxplot comparing mean coral volume (cm^3) ± SE, across three distinct growth morphologies: Branching
323 non-*Acropora* (n = 3), Corymbose, Digitate *Acropora* (n = 5), and Tabular *Acropora* (n = 2)

Precision improved when volume and area calculations were restricted to the upper portion of each skeleton, excluding basal areas and other regions where reconstruction quality was lower.

3.2.3. 3D deviation precision

Replicate reconstructions were also compared using the 3D Compare tool in Geomagic. The lowest variability was observed on corymbose, digitate *Acropora* morphologies with some colonies presenting 2.38 – 4.50% (Table 8). We observed the highest variability on branching non-*Acropora,* with 19.10 % of RSE. Tabular *Acropora* presented RSE values ranging from 6.05 – 10.10%. For more information on the 3D Compare heatmap results used in the precision assessment, see Appendix A.

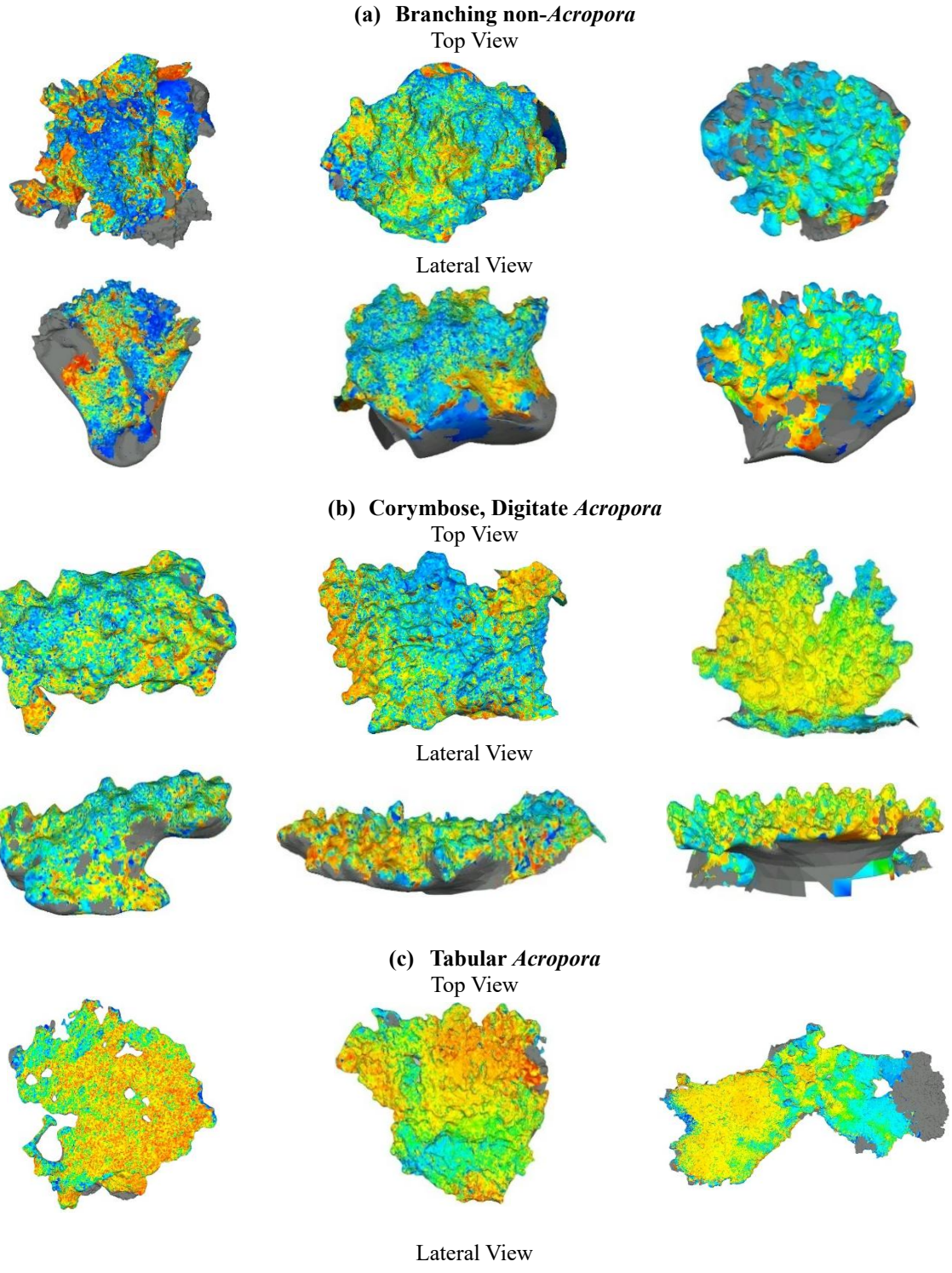
Table 8 Mean Root Square Mean (RMS) measurements for 3 coral morphologies. Values are presented as sample size (n), mean RMS ($\bar{x}$, cm), standard error (SE), and relative standard error (RSE%).

Morpohology	Skeleton	RMS deviation (cm)			
		n	$\bar{x}$	*SE*	*RSE%*
Branching non-*Acropora*	Pdam13	9	0.128	0.0215	19.10
	Pdam64	9	0.193	0.00889	4.65
	Spis22	9	0.240	0.0166	7.04
Corymbose, Digitate *Acropora*	Acor10	9	0.293	0.0201	6.99
	Acor26	9	0.0702	0.00167	2.38
	Acor37.1	9	0.375	0.0399	11.10
	Acor37.2	9	0.106	0.00475	4.50
	Acor55	9	0.684	0.0433	6.59
Tabular *Acropora*	Atab54	9	0.344	0.0334	10.10
	Atab192	9	0.849	0.0506	6.05

3.3. Temporal comparisons between 2022 and 2023 models

The linear mixed-effects model revealed that coral morphology significantly influenced 3D skeletal deviation ($F_{2,51} = 3.31$, $p < 0.05$), with corymbose, digitate and tabular *Acropora* morphologies exhibiting higher deviations compared to the baseline, when using AVET as the response variable. Depth also had a significant effect ($F_{1,51} = 5.70$, $p < 0.05$), with shallower colonies showing reduced deviation. Exposure level did not significantly affect 3D deviation. Random intercepts for reef explained some variability, while site effects were

minimal. On the other hand, the linear mixed-effects model examining 3D deviations with RMS as metric, showed no significant effects of coral morphology ($F_{2,51} = 0.46$, $p > 0.05$), exposure ($F_{3,51} = 0.28$, $p > 0.05$), or depth ($F_{1,51} = 1.67$, $p > 0.05$). Random intercepts for reef and site explained a small amount of variability in RMS deviations.



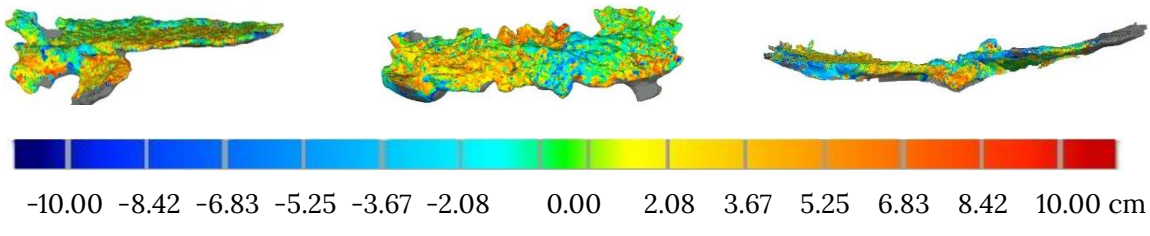


Fig. 5 Heatmaps of 3D reconstruction temporal comparisons (2022–2023) for nine dead corals from three different morphotaxa: (a) Branching non-*Acropora*, (b) Corymbose, Digitate *Acropora*, and (c) Tabular *Acropora*. Each coral colony is shown in top and lateral views. Cool colours indicate areas of negative deviation from 2022-23 (erosion), while warm colours represent positive deviation (surface overgrowth). Grey regions correspond to areas that were not compared, as they were only present in the 2022 reference reconstruction

3.4. Structural metrics

The mixed-effects model examining PCSA found no significant effects of coral morphology ($F_{2,51} = 2.25$, $p > 0.05$), exposure ($F_{3,51} = 0.34$, $p > 0.05$), or depth ($F_{1,51} = 0.92$, $p > 0.05$). Random effects for reef and site explained small variance.

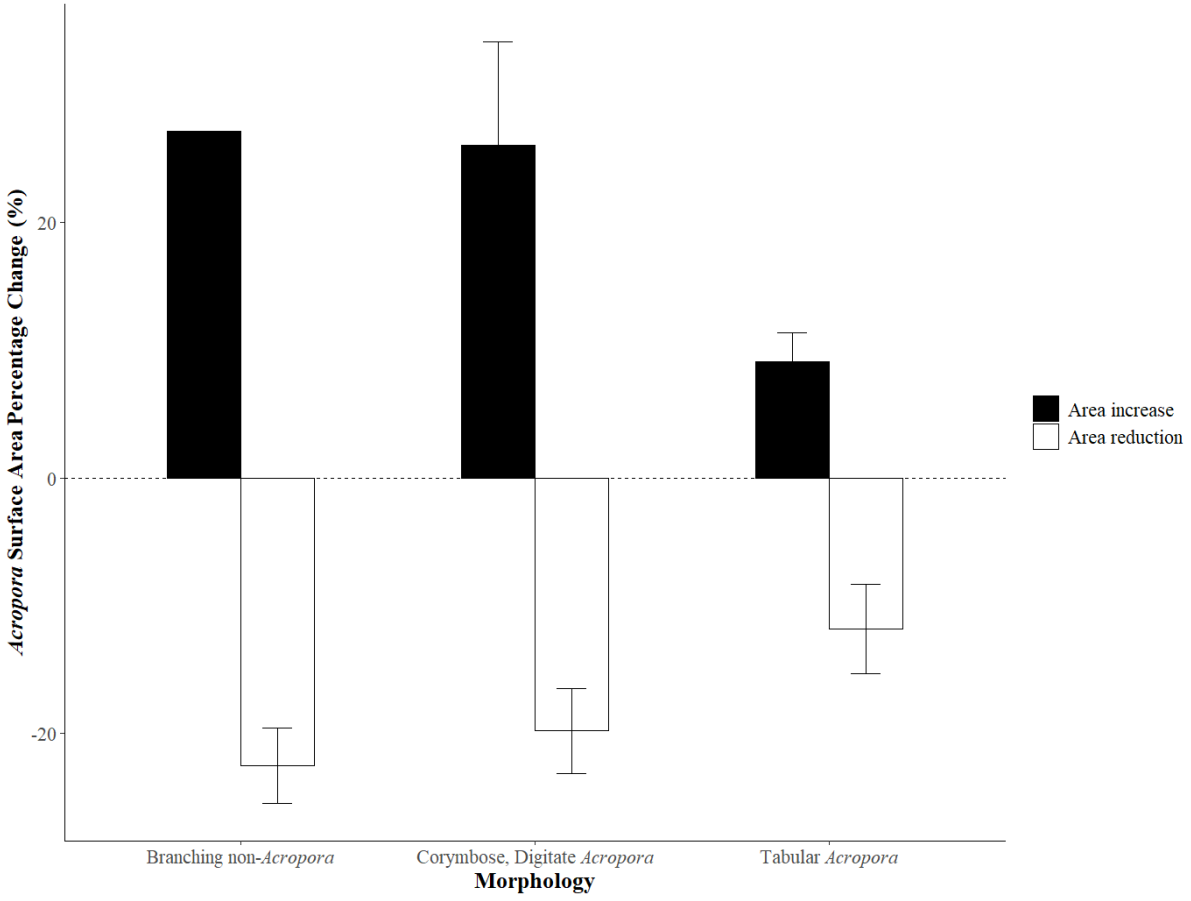


Fig. 6 Bar plot depicting the standardized mean percentage change in surface area between 2022 and 2023 across three morphotaxa. The dashed line represents no change between the years. Positive values indicate an increase in the surface area, while negative values represent a reduction in the surface area. Error bars represent the standard error of the mean (SE), reflecting the variability of the data

The linear mixed-effects model assessing coral volume percentage change (PCV) detected no significant effects of coral morphology ($F_{2,51} = 0.90$, $p > 0.05$), exposure ($F_{3,51} = 0.36$, $p > 0.05$), or depth ($F_{1,51} = 0.10$, $p > 0.05$). A small proportion of variation was explained by differences among sites, but the majority of variation remained unexplained.

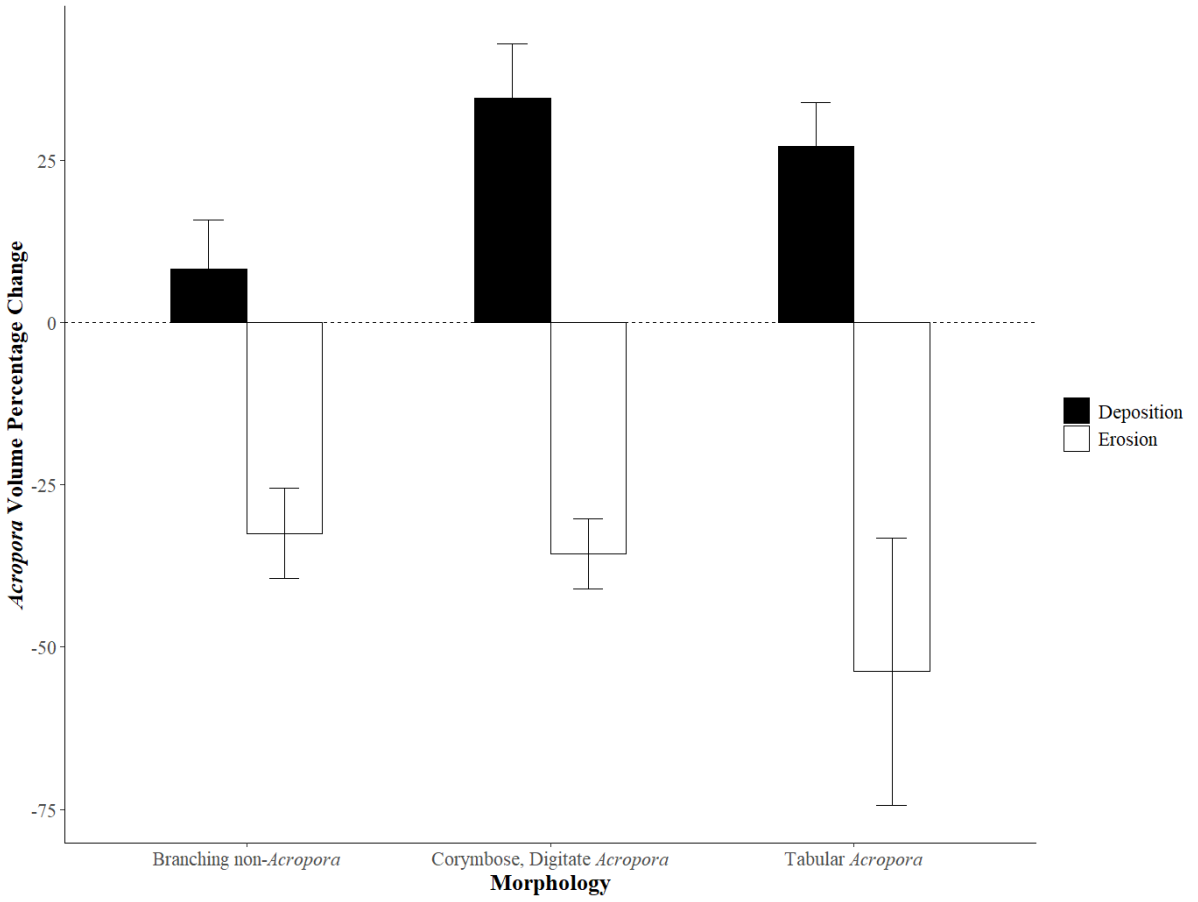


Fig. 7 Bar plot showing the standardized mean percentage change in volume between 2022 and 2023 across three different morphotaxa. The dashed line represents no change between the two years. Positive values indicate surface deposition, while negative values suggest erosion. Error bars represent the standard error of the mean (SE), reflecting the variability of the data

4. DISCUSSION

This study developed and tested a none-invasive workflow for quantifying temporal structural change in dead coral skeletons using image subsets derived from large-area reef photogrammetry. By identifying recently dead coral colonies within reef-scale 3D reconstructions, extracting targeted image sets, and reconstructing individual skeletons at higher resolution, the protocol enabled repeated measurements of colony-level surface area, volume and 3D deviation over a 12-month period. This approach provides a scalable method for tracking post-mortality skeletal dynamics across many colonies, while avoiding destructive sampling.

4.1. Workflow efficiency and methodological precision

The complete workflow for reconstructing individual coral skeletons was 78 minutes per colony, including image filtering, alignment, texture building, and model export (Table 4). Most of this time was computer processing time rather than manual handling time, and several steps can be semi-automated using batch processing in Metashape. Previous studies using similar methodologies have reported processing times ranging from 15 to 70 minutes (Ferrari et al., 2017a; Lange & Perry, 2020). However, processing time can vary significantly depending on coral morphology, with small-massive, and simpler structures requiring only 10 to 20 minutes, while larger, more complex species can take several hours to process (Aston et al., 2022)..

The precision assessment showed that the workflow produced repeatable estimates of skeletal volume and surface area, although precision varied among colonies and morphologies. Relative standard error values were generally low for volume and surface area, indicating that the method can reliably detect colony-level structural metrics when reconstructions are of sufficient quality. The average 3D deviation between the two versions in the precision assessment was 0.21 cm, with a standard deviation of 1.18 cm (Fig. 2). This variability is likely due to uncertainty in the bottom portion of the coral, which was poorly photographed, as the images used for reconstruction were captured at a plot-level scale (Fig. 2). However, when using the Compute Volume to Plan tool to calculate only the upper portion of the coral, excluding the gray and uncertain areas, the difference in 3D volume between the two skeleton versions was just 1.07% or 2,472 cm^3. Previous studies have assessed their precision by running a repeated modeling, which helps define a coefficient of variations (CV) between the different versions of the model, reporting values between 1 and 10% (Ferrari et al., 2017a; Figueira et al., 2015; Million et al., 2021). Figueira et al. (2015) suggested that precision is highly variable depending on the morphology of the coral, with small-massive corals being the most precise, while bottlebrush corals being remain as the least precise. Lateral and top views show a high degree of alignment between the two versions, whereas the bottom view highlights

uncertain regions (grey areas) that could not be accurately compared. These uncertainties stem from the use of plot-scale images rather than colony-scale images, emphasising the need for more scale-specific approaches in studies requiring higher precision, and further investigations on morphology effect on structural changes (Fig. 1).

4.2. Post-mortality structural change among coral morphologies

Temporal comparisons between 2022 and 2023 showed that dead coral skeletons underwent measurable structural change within the first year after mortality. 3D deviation heatmaps indicated that individual skeletons often contained both areas of apparent surface loss and areas of apparent surface gain, consistent with the simultaneous action of erosion, fragmentation, surface deposition and biological overgrowth. These patterns demonstrate that post-mortality change is not simply a uniform reduction in skeletal volume, but a spatially heterogeneous process occurring across different parts of the colony surface.

Coral morphotaxa influenced average 3D deviation, suggesting skeletal morphology affects the direction and distribution of early post-mortality surface change. Branching non-*Acropora* skeletons appeared particularly susceptible to surface loss in first year after mortality (Fig. 3), which might reflect their finer branches, more delicate skeletal architecture or greater vulnerability to grazing or breakage. However, percentage change in volume and surface area did not show significant differences among morphotaxa. This suggests that 3D deviation metrics may be more sensitive to localised surface change than whole-colony summary metrics such as total volume or surface area.

The relationship between volume change and surface area change was also complex. A decrease in coral volume is consistent with bioerosion or material loss, whereas surface area may increase at the same time if bioerosion, fragmentation or surface roughening creates additional holes, cavities or exposed surfaces (Fig. 3c). Because this method quantifies only external structural change, it cannot distinguish among all these processes directly, nor can it measure internal erosion or changes in skeletal density. The results should therefore be interpreted as changes in external 3D structure, rather than direct measurements of total carbonate loss.

4.3. Comparison with previous studies

The findings of this study are consistent with previous research showing that dead coral skeletons can undergo rapid structural alteration after mortality. Ferrari et al. (2017), looked at shrinkage of tabular *Acropora*, with colony focus imaging, reporting a volume and surface area decreased of 52% and 47%, respectively. In the present study, volumetric declines were of a similar order of magnitude, suggesting that our plot-derived can

provide robust and reliable estimates of volume change. However, reductions in surface area were smaller than those reported in colony-focused imaging studies, which may indicate that surface area is more sensitive to image resolution, model completeness and the ability to capture fine-scale skeletal features. Further methodological refinement may be necessary to improve the precision and sensitivity of surface area estimates.

4.4. Environmental effects and monitoring implications

Differences in structural changes across exposure categories were minimal, suggesting that early stages of external erosion and surface deposition are primarily influenced by the morphology of the skeleton. Previous studies have reported higher rates of both external and internal bioerosion in coral blocks located in more exposed reef zones, such as reef slopes, compared to more sheltered areas like reef lagoons (Silbiger et al., 2017; Thomson et al., 2024). However, most of these studies used experimental coral blocks and longer deployment periods, often exceeding 12 months (Enochs et al., 2016; Kiene & Hutchings, 1994; Pari et al., 2002). It is possible that stronger exposure-related patterns emerge over longer periods, once grazing, boring, fragmentation and dissolution processes have had more time to accumulate.

Structural complexity is a fundamental determinant of reef health and biodiversity, influencing recruitment of reef associated species and habitat availability (Alvarez-Filip et al., 2009; Graham & Nash, 2013). Although, volume reduction indicates external bioerosion, the observed increase in surface area for some morphotaxa, suggests that at least in early stages (<1 year), bioerosion and fragmentation may enhance habitat complexity through the formation of tunnels or small cavities. However, we also observed a considerable increase in volume for all morphologies, probably due to surface deposition of algae or other benthic organisms (Diaz-Pulido & McCook, 2004; Glynn & Manzello, 2015; Nugues & Roberts, 2003). These findings highlight the importance of monitoring dead colonies over longer periods (>1 year) to better understand coral reef dynamics and overall ecosystem health. For instance, Chazottes et al. (1995) reported that external bioerosion, measured as percentage of volume change, nearly tripled after two years of experimentation compared to values recorded after one year, suggesting that bioerosion exponentially increases over time.

Tracking these changes is important because dead coral skeletons continue to contribute to reef habitat structure after coral mortality. In the short term, erosion, fragmentation and surface roughening may create holes, cavities and refuges for small reef organisms. Over longer timescales, however, continued skeletal breakdown can reduce reef topographical complexity, carbonate structure and habitat availability. Quantifying the rate and

trajectory of this transition is therefore critical for understanding how reef degradation affects habitat structure and ecosystem function.

Conclusions

This study demonstrates the value of photogrammetry and 3D reconstruction as powerful, precise and non-invasive tools for quantifying structural change in coral skeletons. The workflow provides repeatable estimates of volume, surface area and 3D deviation, particularly when analyses are restricted to well-reconstructed portions of the skeleton. Although limitations related to image resolution, basal coverage and filtering uncertainty can influence accuracy, these can be partly mitigated though methodological refinements and standardisation.

By enabling many recently dead colonies to be tracked non-destructively across repeated surveys, this approach provides a scalable tool for assessing reef degradation processes. Future work incorporating longer time series, broader taxonomic coverage, targeted validation imagery and complementary measures of internal bioerosion or skeletal density will further advance our understanding of coral skeletal dynamics after mortality. Integrating 3D modelling into long-term reef monitoring programmes could help researchers and managers better quantify changes in reef structure, habitat complexity and recovery potential under increasing disturbance, supporting improved conservation and management of the Great Barrier Reef and other coral reef systems.

REFERENCES

Alvarez-Filip, L., Dulvy, N. K., Gill, J. A., Côté, I. M., & Watkinson, A. R. (2009). Flattening of Caribbean coral reefs: Region-wide declines in architectural complexity. *Proceedings of the Royal Society B: Biological Sciences*, *276*(1669), 3019–3025. https://doi.org/10.1098/rspb.2009.0339

Álvarez-Noriega, M., Aston, E. A., Becker, M., Fabricius, K. E., Figueira, W. F., Gordon, S. E., Krensel, R., Lechene, M. A., Remmers, T., Toor, M., & Ferrari, R. (2025). Challenging Paradigms Around the Role of Colony Size, Taxa, and Environment on Bleaching Susceptibility. *Global Change Biology*, *31*(2), e70090. https://doi.org/10.1111/gcb.70090

Aston, E. A., Duce, S., Hoey, A. S., & Ferrari, R. (2022). A Protocol for Extracting Structural Metrics From 3D Reconstructions of Corals. *Frontiers in Marine Science*, *9*. https://doi.org/10.3389/fmars.2022.854395

Bates, D., Mächler, M., Bolker, B., & Walker, S. (2015). Fitting Linear Mixed-Effects Models Using **lme4**. *Journal of Statistical Software*, *67*(1). https://doi.org/10.18637/jss.v067.i01

Bruno, J. F., & Selig, E. R. (2007). Regional decline of coral cover in the Indo-Pacific: Timing, extent, and subregional comparisons. *PLoS ONE*, *2*(8). https://doi.org/10.1371/journal.pone.0000711

Chazottes, V., Campion-Alsumard, T. L., & Peyrot-Clausade, M. (1995). Bioerosion rates on coral reefs: Interactions between macroborers, microborers and grazers (Moorea, French Polynesia). *Palaeogeography, Palaeoclimatology, Palaeoecology*, *113*(2–4), 189–198. https://doi.org/10.1016/0031-0182(95)00043-L

Deaker, D. J., & Byrne, M. (2022). Crown of thorns starfish life-history traits contribute to outbreaks, a continuing concern for coral reefs. *Emerging Topics in Life Sciences*, *6*(1), 67–79. https://doi.org/10.1042/ETLS20210239

Diaz-Pulido, G., & McCook, L. J. (2004). *Effects of live coral, epilithic algal communities and substrate type on algal recruitment*. *23*, 225–233.

Eakin, C. M. (2001). *A tale of two Enso Events: Carbonate budgets and the influence of two warming disturbances and intervening variability, Uva Island, Panama*. Bulletin of Marine Science. *69*(1).

Enochs, I. C., Manzello, D. P., Kolodziej, G., Noonan, S. H., Valentino, L., & Fabricius, K. E. (2016). Enhanced macroboring and depressed calcification drive net dissolution at high-CO2 coral reefs. *Proceedings of the Royal Society B: Biological Sciences*.

Estrada-Saldívar, N., Molina-Hernández, A., Pérez-Cervantes, E., Medellín-Maldonado, F., González-Barrios, F. J., & Alvarez-Filip, L. (2020). Reef-scale impacts of the stony coral tissue loss disease outbreak. *Coral Reefs*, *39*(4), 861–866. https://doi.org/10.1007/s00338-020-01949-z

Ferrari, R., Figueira, W. F., Pratchett, M. S., Boube, T., Adam, A., Kobelkowsky-Vidrio, T., Doo, S. S., Atwood, T. B., & Byrne, M. (2017a). 3D photogrammetry quantifies growth and external erosion of individual coral colonies and skeletons. *Scientific Reports*, *7*(1). https://doi.org/10.1038/s41598-017-16408-z

Ferrari, R., Figueira, W. F., Pratchett, M. S., Boube, T., Adam, A., Kobelkowsky-Vidrio, T., Doo, S. S., Atwood, T. B., & Byrne, M. (2017b). 3D photogrammetry quantifies growth and external erosion of individual coral colonies and skeletons. *Scientific Reports*, *7*(1), 16737. https://doi.org/10.1038/s41598-017-16408-z

Figueira, W., Ferrari, R., Weatherby, E., Porter, A., Hawes, S., & Byrne, M. (2015). Accuracy and precision of habitat structural complexity metrics derived from underwater photogrammetry. *Remote Sensing*, *7*(12), 16883–16900. https://doi.org/10.3390/rs71215859

Fox, J., & Weisberg, S. (2023). *car: Companion to Applied Regression*. https://cran.r-project.org/package=car

Glynn, P. W., & Manzello, D. P. (2015). Bioerosion and Coral Reef Growth: A Dynamic Balance. In C. Birkeland (Ed.), *Coral Reefs in the Anthropocene* (pp. 67–97). Springer Netherlands. https://doi.org/10.1007/978-94-017-7249-5_4

Gordon, S., Aston, E., Lechene, M., Harianto, J., Figueira, W., Gonzalez Rivero, M., & Ferrari, R. (2023). *Field photogrammetry in 4D. Reef Restoration and Adaption Program (EcoRRAP). Standard Operational Procedure Number 1: Overview and in-field workflow.* Australian Institute of Marine Science. https://doi.org/10.25845/SE7T-PS86

Gordon, S., Aston, E., Lechene, M., Remmers, T., Piccaluga, A., Brinker, E., Cowasji, Z., Harianto, J., Bray, P., Millar, G., Watkin, B., Figueira, W., Gonzalez Rivero, M., & Ferrari Legorreta, R. (2024). *Field photogrammetry in 4D: Model Processing. Reef Restoration and Adaption Program (EcoRRAP). Standard Operational Procedure 15 (2 of series): Model processing.* (p. 57). Australian Institute of Marine Science. https://doi.org/10.25845/mwkv-ez70

Graham, N. A. J., & Nash, K. L. (2013). The importance of structural complexity in coral reef ecosystems. *Coral Reefs*, *32*(2), 315–326. https://doi.org/10.1007/s00338-012-0984-y

Hughes, T. P., Bellwood, D. R., Baird, A. H., Brodie, J., Bruno, J. F., & Pandolfi, J. M. (2011). Shifting base-lines, declining coral cover, and the erosion of reef resilience: Comment on Sweatman et al. (2011). *Coral Reefs*, *30*(3), 653–660. https://doi.org/10.1007/s00338-011-0787-6

Hughes, T. P., Kerry, J. T., Álvarez-Noriega, M., Álvarez-Romero, J. G., Anderson, K. D., Baird, A. H., Babcock, R. C., Beger, M., Bellwood, D. R., Berkelmans, R., Bridge, T. C., Butler, I. R., Byrne, M., Cantin, N. E., Comeau, S., Connolly, S. R., Cumming, G. S., Dalton, S. J., Diaz-Pulido, G., … Wilson, S. K. (2017). Global warming and recurrent mass bleaching of corals. *Nature*, *543*(7645), 373–377. https://doi.org/10.1038/nature21707

Kiene, W. E., & Hutchings, P. A. (1994). Bioerosion experiments at Lizard Island, Great Barrier Reef. *Coral Reefs*, *13*(2), 91–98. https://doi.org/10.1007/BF00300767

Kopecky, K. L., Holbrook, S. J., Partlow, E., Cunningham, M., & Schmitt, R. J. (2024). Changing disturbance regimes, material legacies, and stabilizing feedbacks: Dead coral skeletons impair key recovery processes following coral bleaching. *Global Change Biology*, *30*(9), e17504. https://doi.org/10.1111/gcb.17504

553 Lange, I. D., & Perry, C. T. (2020). A quick, easy and non-invasive method to quantify coral growth rates using
554 photogrammetry and 3D model comparisons. *Methods in Ecology and Evolution*, *11*(6), 714–726.
555 https://doi.org/10.1111/2041-210X.13388
556 Marsden, A., Bentley, J., Tuffley, K., Reichelt, R., Fitzgerald, S., & Roberts, S. (2017). *Andrew Fyffe Finance*
557 *Officer Great Barrier Reef Foundation Chairman and Chief Executive Great Barrier Reef Marine Park*
558 *Authority*.
559 Million, W. C., O'Donnell, S., Bartels, E., & Kenkel, C. D. (2021). Colony-Level 3D Photogrammetry Reveals
560 That Total Linear Extension and Initial Growth Do Not Scale With Complex Morphological Growth in
561 the Branching Coral, Acropora cervicornis. *Frontiers in Marine Science*, *8*.
562 https://doi.org/10.3389/fmars.2021.646475
563 Molina-Hernández, A., Medellín-Maldonado, F., Lange, I. D., Perry, C. T., & Álvarez-Filip, L. (2022). Coral
564 reef erosion: In situ measurement on different dead coral substrates on a Caribbean reef. *Limnology and*
565 *Oceanography*, *67*(12), 2734–2749. https://doi.org/10.1002/lno.12234
566 Nugues, M. M., & Roberts, C. M. (2003). Coral mortality and interaction with algae in relation to
567 sedimentation. *Coral Reefs*, *22*(4), 507–516. https://doi.org/10.1007/s00338-003-0338-x
568 Ogle, D. H., Doll, J. C., & Wheeler, A. P. (2024). *FSA: Fisheries Stock Assessment Methods and Data*.
569 https://fishr-core-team.github.io/FSA/
570 Pari, N., Peyrot-Clausade, T., & Hutchings, P. A. (2002). *Bioerosion of experimental substrates on high islands*
571 *and atoll lagoons (French Polynesia) during 5 years of exposure*. *279*, 109–127.
572 https://doi.org/10.1016/S00220981(02)00243-5
573 Perry, C. T., Murphy, G. N., Kench, P. S., Smithers, S. G., Edinger, E. N., Steneck, R. S., & Mumby, P. J. (2013).
574 Caribbean-wide decline in carbonate production threatens coral reef growth. *Nature Communications*,
575 *4*. https://doi.org/10.1038/ncomms2409
576 Remmers, T., Boutros, N., Wyatt, M., Gordon, S., Toor, M., Roelfsema, C., Fabricius, K., Grech, A., Lechene,
577 M., & Ferrari, R. (2025). RAPIDBENTHOS: Automated segmentation and multi-view classification of
578 coral reef communities from photogrammetric reconstruction. *Methods in Ecology and Evolution*,
579 *16*(2), 427–441. https://doi.org/10.1111/2041-210X.14477
580 Risk, M. J. (1972). *Fish diversity on a coral reef in the Virgin Islands*. (153).
581 https://doi.org/https://doi.org/10.5479/si.00775630.153.1

Silbiger, N. J., Donahue, M. J., & Brainard, R. E. (2017). Environmental drivers of coral reef carbonate production and bioerosion: A multi-scale analysis. *Ecology*, *98*(10), 2547–2560. https://doi.org/10.1002/ecy.1946

Taylor, B. M., Benkwitt, C. E., Choat, H., Clements, K. D., Graham, N. A. J., & Meekan, M. G. (2020). Synchronous biological feedbacks in parrotfishes associated with pantropical coral bleaching. *Global Change Biology*, *26*(3), 1285–1294. https://doi.org/10.1111/gcb.14909

Thomson, D. P., Dee, S., Doropoulos, C., Orr, M., Wilson, S. K., & Hoey, A. S. (2024). High rates of erosion on a wave-exposed fringing coral reef. *Limnology and Oceanography*, *69*(6), 1439–1449. https://doi.org/10.1002/lno.12586

Toor, M., Lechene, M., Becker, M. L., Remmers-Barry, T., Gordon, S., Stratford, J., & Ferrari, R. (2025). *Field Photogrammetry in 4D: Digitisation and 2D metric extraction. Reef Restoration and Adaptation Program (EcoRRAP). Standard Operating Procedure 17 (No. 3 of series).* (p. 77). Australian Institute of Marine Science.

Wickham, H., & Bryan, J. (2024). *readxl: Read Excel Files*. Posit, PBC. https://readxl.tidyverse.org

Wickham, H., Chang, W., Henry, L., Takahashi, K., Wilke, C., Woo, K., Yutani, H., Dunnington, D., & Brand, T. van den. (2024). *ggplot2: Create Elegant Data Visualisations Using the Grammar of Graphics*. Posit, PBC. https://ggplot2.tidyverse.org

Wickham, H., François, R., Henry, L., Müller, K., & Vaughan, D. (2023). *dplyr: A Grammar of Data Manipulation*. Posit Software, PBC. https://dplyr.tidyverse.org

Wickham, H., Vaughan, D., & Girlich, M. (2023). *tidyr: Tidy Messy Data*. Posit Software, PBC. https://tidyr.tidyverse.org

Supplementary Files

This is a list of supplementary files associated with this preprint. Click to download.

- CRsupplementary2026.docx